Optimal Pilot Waveform Assisted Modulation for Ultrawideband Communications

Liuqing Yang, *Student Member, IEEE,* and Georgios B. Giannakis, *Fellow, IEEE*

***Abstract*—Ultrawideband (UWB) transmissions induce pronounced frequency-selective fading effects in their multipath propagation. Multipath diversity gains can be collected to enhance performance, provided that the underlying channel can be estimated at the receiver. To this end, we develop a novel pilot waveform assisted modulation (PWAM) scheme that is tailored for UWB communications. We select our PWAM parameters by jointly optimizing channel estimation performance and information rate. The resulting transmitter design maximizes the average capacity, which is shown to be equivalent to minimizing the mean-square channel estimation error, and thereby achieves the Cramér–Rao lower bound. Application of PWAM to practical UWB systems is promising because it entails simple integrate-and-dump operations at the frame rate. Equally important, it offers a flexible UWB channel estimator, capable of striking desirable rate-performance tradeoffs depending on the channel coherence time.**

***Index Terms*—Channel estimation, impulse radio, multipath fading channels, time-hopping, transmitted reference (TR), ultrawideband (UWB) systems.**

I. Introduction

THERE HAS been growing interest toward ultrawideband (UWB) systems for short range indoor wireless communications [5], [18]. Conveying information with ultrashort pulses, UWB transmissions can resolve many paths, and are, thus, rich in multipath diversity. Collecting the latter requires Rake receivers with a large number of fingers [4], [19]. As Rake reception relies on channel knowledge, UWB channel estimation is also challenging [10]. Moreover, each of the resolvable waveforms undergoes a different channel, which causes distortion in the received pulse shape [16], and renders usage of an ideal line-of-sight path signal as a template suboptimal.

To improve template matching performance, an old (see, e.g., [15]) transmitted reference (TR) spread spectrum scheme was advocated recently in [6], and its performance was analyzed in [3]. The TR signalling scheme couples each information-conveying pulse with an unmodulated reference (a.k.a. pilot) pulse. The received pilot pulses are averaged, and used as the correlator template to decode the received information-bearing pulses. As half of the transmitted pulses are always used as pilots in TR, regardless of the channel, the information rate drops by 50%.

Manuscript received July 4, 2002; revised January 3, 2003 and March 3, 2003; accepted May 6, 2003. The editor coordinating the review of this paper and approving it for publication is A. Scaglione. This work was presented in part at the 36th Asilomar Conference on Signals, Systems, and Computers, Pacific Grove, CA, November 2002.

The authors are with the Department of Electrical and Computer Engineering, University of Minnesota, Minneapolis, MN 55455 USA (e-mail: georgios@ece.umn.edu).

Digital Object Identifier 10.1109/TWC.2004.830827

In this paper, we introduce a general pilot waveform assisted modulation (PWAM) scheme, which subsumes TR as a special case. To account for both performance and bandwidth efficiency, we design our PWAM to minimize the channel's mean-square estimation error (MSE), and maximize the average capacity. The resulting PWAM designs optimally balance channel estimation performance and information rate. Tailoring our optimal PWAM for UWB-specific needs, we also develop an optimal (so-termed ES-PWAM) scheme, which features pilot and information pulses with equal signal-to-noise ratios (SNRs). PWAM is applicable to both pulse amplitude modulation (PAM), and pulse position modulation (PPM) [9], [14], [18], [21]. In this paper, we focus on PAM for simplicity, though the analysis carries over to PPM as well.

Our PWAM for UWB is reminiscent of the pilot symbol assisted modulation (PSAM), which was originally developed for bandlimited time-selective channels [2], and has recently been extended to narrowband frequency-selective channels [1], [12]. Although both aim at training-based channel estimation, they differ in several aspects as follows:

1) PSAM applies to narrowband channels with intersymbol interference (ISI), whereas PWAM estimates UWB channels that entail no-ISI;
2) PSAM estimates the taps of discrete-time equivalent frequency-selective channels, whereas PWAM recovers the equivalent continuous-time channel waveform;
3) corresponding to one pilot symbol used in PSAM, PWAM allocates multiple pilot pulses across frames, and is, thus, more flexible to strike desirable rate-performance tradeoffs arising with variable channel coherence time.

As far as practical UWB receiver design issues, the most attractive feature of PWAM is that it relies only on frame-rate samples, which are acquired via simple integrate-and-dump operations. This is to be contrasted with approaches that (like PSAM) attempt to estimate the discrete-time equivalent channel taps, and require $10 - 25$ samples per monocycle[1] pulse [10].

The rest of this paper is organized as follows. The system model is given in Section II. Section III derives the channel estimator, and the associated channel MSE. In Section IV, the average capacity is given in closed form, based on which the optimal parameters of our PWAM are derived. Our two criteria, namely channel MSE and average capacity, are linked in this section by showing that minimizing the former is equivalent to maximizing the latter. In Section V, modifications are carried out

[1]Such an oversampling with a typical monocycle duration of 0.7 ns leads to a formidable sampling rate of 14.3–35.7 GHz, not to mention the huge number of channel taps that must be estimated.

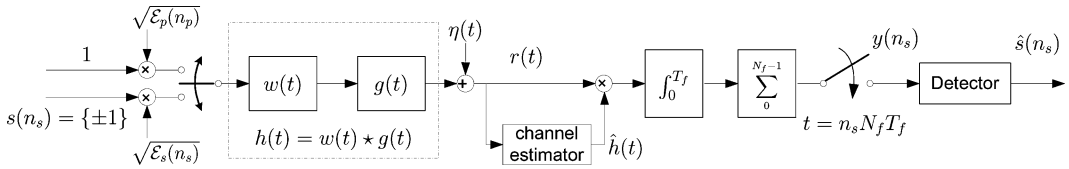

Fig. 1. System block diagram.

to further tailor our optimal PWAM to UWB communications. Simulations and comparisons are presented in Section VI.

II. System Model

Consider a peer-to-peer UWB communication system, where binary information symbols are conveyed by a stream of ultrashort pulses. The transmit-pulse $w(t)$ has typical duration T_w between 0.2–2 ns. To transmit one binary ± 1 symbol, such ultrashort (impulse-like) pulses are repeated over N_f consecutive frames, each of duration T_f.

As shown in Fig. 1, the overall channel $h(t)$ comprises the convolution of the pulse shaper $w(t)$ with the physical multipath channel $g(t) := \sum_{l=0}^{L-1} \gamma_l \delta(t-\tau_l)$, where L denotes the number of propagation paths, γ_l and τ_l are the attenuation, and the delay associated with the lth path. With T_g denoting the maximum delay spread of the dense multipath channel, UWB systems avoid ISI by simply choosing $T_f > T_g + T_w$.

We model the multipath channel in an indoor environment as quasi-static. Specifically, we suppose that γ_l and τ_l, and thus, $h(t)$, remain invariant over a burst of duration $\bar{N}T_f$ seconds, but may change from burst to burst. Each burst includes up to $N := \bar{N}/N_f$ symbols that are either training or information-bearing. During each burst, N_s distinct information symbols are transmitted. In other words, $\bar{N}_s := N_s N_f$ out of the total of $\bar{N}$ transmitted pulses of each burst are information-conveying. Consequently, the number of training (pilot) pulses is given by $\bar{N}_p = \bar{N} - \bar{N}_s$. Clearly, the number of symbols (information and pilot) per burst satisfies $N = N_s + N_p$, where $N_p := \bar{N}_p/N_f$ can be interpreted as the number of pilots per burst,[2] but is not necessarily an integer.

Supposing that coarse timing has been acquired as in [17] and [22], an estimate of the composite channel $h(t)$ can be formed based on the received pilot waveforms. This estimate $\hat{h}(t)$ is then used as the correlator template to decode the received information-conveying waveforms, as illustrated in Fig. 1. Increasing the energy and/or the number of pilot waveforms improves the reliability of $\hat{h}(t)$, which facilitates collection of the channel-induced multipath diversity. On the other hand, it also reduces the energy and/or the number of information waveforms, and thus, hauls back the information rate.

Our *objective* is to design PWAM transmissions which optimize not only the channel estimation performance, but also the information rate. To be more specific, we seek to optimize the placement, the number, and the energy allocation of pilot waveforms (pulses).

[2]As a mnemonic rule, quantities with overbar (e.g., $\bar{N}$) are obtained by multiplying their counterparts without overbar (e.g., N) by the number of frames per symbol (N_f); i.e., $\bar{N} = NN_f$.

III. Channel Estimator and Channel MMSE

In this section, we will derive a UWB channel estimator based on $\bar{N}_p$ pilot waveforms. Let $\mathcal{E}_p$ denote the total energy assigned to pilot waveforms. With $\mathcal{E}_p(n_p)$ denoting the energy of the n_pth pilot waveform, we have $\mathcal{E}_p = \sum_{n_p=0}^{\bar{N}_p-1} \mathcal{E}_p(n_p)$. The received waveform corresponding to the n_pth pilot pulse is

$$r_{n_p}(t) = \sqrt{\mathcal{E}_p(n_p)}h(t) + \eta_{n_p}(t),\ t \in [0, T_f) \tag{1}$$

for all $n_p \in [0, \bar{N}_p - 1]$, where $\eta_{n_p}(t)$ denotes zero-mean additive Gaussian noise (AGN) in the frame containing the n_pth pilot waveform. Let the receiver frontend be modeled as an ideal bandpass filter with double-sided bandwidth B ($\gg 1/T_f$) and center frequency f_0. The AGN $\eta(t)$ across frames (pilot or data) is bandpass filtered white Gaussian noise with double-sided power spectral density $\sigma^2/2$, and autocorrelation function

$$R_\eta(\tau) := E[\eta(t)\eta(t+\tau)] = \sigma^2 B \mathrm{sinc}(B\tau)\cos(2\pi f_0 \tau) \tag{2}$$

where $\mathrm{sinc}(t) := \sin(\pi t)/(\pi t)$.

A total of $\bar{N}_p$ received pilot waveforms are summed up to form the channel estimate

$$\hat{h}(t) = \beta \sum_{n_p=0}^{\bar{N}_p-1} r_{n_p}(t) = \beta \sum_{n_p=0}^{\bar{N}_p-1} \left[\sqrt{\mathcal{E}_p(n_p)}h(t) + \eta_{n_p}(t)\right] \tag{3}$$

for $t \in [0, T_f)$, where the sum is premultiplied by a constant $\beta := \left(\sum_{n_p=0}^{\bar{N}_p-1} \sqrt{\mathcal{E}_p(n_p)}\right)^{-1}$ to guarantee the unbiasedness of $\hat{h}(t)$. Later on, we will show that this simple estimator that amounts to an equal gain combiner (EGC) achieves the Cramér–Rao lower bound (CRLB), provided that the energy is distributed properly among pilot waveforms $\{\mathcal{E}_p(n_p)\}_{n_p=0}^{\bar{N}_p-1}$.

Defining the channel estimation error as $\tilde{h}(t) := \hat{h}(t) - h(t)$, we find that its mean is $E[\tilde{h}(t)] = 0$, and its autocorrelation function is given by: $E[\tilde{h}(t)\tilde{h}(t+\tau)] = \beta^2 \sum_{n_p=0}^{\bar{N}_p-1} \sum_{m_p=0}^{\bar{N}_p-1} E[\eta_{n_p}(t)\eta_{m_p}(t+\tau)]$. With pilot waveforms being separated by at least one information-conveying waveform, and taking into account that $B \gg 1/T_f$, we deduce that [cf. (2)]

$$E[\eta_{n_p}(t)\eta_{m_p}(t+\tau)] \approx R_\eta(\tau)\delta(m_p - n_p) \quad \forall \tau \in (-T_f, T_f), \text{and } m_p, n_p \in [0, \bar{N}_p - 1] \tag{4}$$

where $\delta(\cdot)$ stands for Kronecker's delta function: $\delta(k) = 1$ for $k = 0$. It follows that $\forall \tau \in (-T_f, T_f)$

$$E[\tilde{h}(t)\tilde{h}(t+\tau)] = \bar{N}_p \beta^2 \sigma^2 B \mathrm{sinc}(B\tau)\cos(2\pi f_0 \tau). \tag{5}$$

Evaluating (5) for $\tau = 0$ yields $E[\tilde{h}^2(t)] = \bar{N}_p\beta^2\sigma^2 B$. For notational convenience, we define the normalized MSE of $\hat{h}(t)$ as

$$\sigma^2_{\hat{h}} := \frac{E[\tilde{h}^2(t)]}{B} = \bar{N}_p\beta^2\sigma^2. \tag{6}$$

Equations (3) and (6) suggest that for a given $\mathcal{E}_p$ and a fixed energy distribution among pilot waveforms $\{\mathcal{E}_p(n_p)\}_{n_p=0}^{\bar{N}_p-1}$, the placement of pilot waveforms per transmitted burst neither affects the constant β, nor the MSE $\sigma^2_{\hat{h}}$. Hence, from an estimation point of view, the placement of pilot waveforms does not affect $\hat{h}(t)$, so long as the channel remains invariant over the burst. However, different placements benefit different aspects of the overall system design. For instance, inserting the pilot waveforms equi-spaced throughout a burst is beneficial especially when the channel is varying slowly over time, while gathering all pilot waveforms at the beginning of each burst (preamble) will yield the smallest delay in symbol decoding.

With regards to the energy distribution among pilot waveforms which yields the minimum MSE $\sigma^2_{\hat{h}}$, we have the following result.

Proposition 1: Given the total number of pilot waveforms per burst $\bar{N}_p$, and the total energy $\mathcal{E}_p$ assigned to them, equi-powered pilot waveforms minimize the MSE in channel estimation. The resulting $\beta = 1/\sqrt{\bar{N}_p\mathcal{E}_p}$ yields the channel MMSE

$$\sigma^2_{\hat{h}} = \frac{\sigma^2}{\mathcal{E}_p}. \tag{7}$$

Proof: For a fixed $\bar{N}_p$, minimizing $\sigma^2_{\hat{h}}$ in (6) is equivalent to minimizing β, subject to the fixed total pilot energy $\mathcal{E}_p = \sum_{n_p=0}^{\bar{N}_p-1}\mathcal{E}_p(n_p)$. Using the Lagrange multiplier method, it can be readily shown that β is minimized if and only if $\mathcal{E}_p(n_p) = \mathcal{E}_p/\bar{N}_p, \forall n_p \in [0, \bar{N}_p - 1]$. It follows that

$$\beta = \frac{1}{\bar{N}_p\sqrt{\frac{\mathcal{E}_p}{\bar{N}_p}}} = \frac{1}{\sqrt{\bar{N}_p\mathcal{E}_p}}.$$

Substituting β into (6) yields the channel MMSE

$$\sigma^2_{\hat{h}} = \left(\frac{1}{\sqrt{\bar{N}_p\mathcal{E}_p}}\right)^2 \sigma^2\bar{N}_p = \frac{\sigma^2}{\mathcal{E}_p}.$$

■

This result is not surprising, since with equi-powered pilot waveforms, the estimator given in (3) is nothing but a least squares (LS) estimator, which for the model in (1) is optimal in the maximum likelihood (ML) sense, and thus, achieves the CRLB (see, e.g., [7, Ch. 8]). Instead of the EGC in (3), one may be tempted to consider a maximum ratio combiner, which being the counterpart of a weighted LS estimator, offers ML optimality even with nonequi-powered pilot pulses. However, equi-powered pilot pulses are well motivated by their low peak-to-average power ratios.

Equation (7) implies that as $\mathcal{E}_p$ increases, the channel MMSE decreases monotonically. On the other hand, for a fixed total transmission energy per burst $\mathcal{E} = \mathcal{E}_s + \mathcal{E}_p$, the energy assigned to information symbols $\mathcal{E}_s$ decreases with increasing $\mathcal{E}_p$. The optimal $\mathcal{E}_p$ is not yet obvious from the preceding analysis. Furthermore, we deduce from (7) the channel MMSE depends on $\mathcal{E}_p$, but not on the number of pilot waveforms $\bar{N}_p$. To find the optimal $\bar{N}_p$ and the optimal $\mathcal{E}_p$ subject to a fixed burst size N, and total energy per burst $\mathcal{E}$, we need a criterion capturing information rate aspects.

IV. Average Capacity

Toward this objective, we will use the average capacity C conditioned on our overall system model depicted in Fig. 1. Different from Shannon's capacity, C depends also on the receiver structure, and provides a metric of both performance and information rate achievable by our UWB system with channel estimation, correlator reception, and decoding.

As mentioned earlier, the placement of pilot waveforms does not affect the performance of our channel estimator, and thus, the decoding stage that depends on it. In the analysis hereafter, we will assume that all pilot waveforms are gathered at the end of each burst for notational simplicity.

To reach a closed form expression for the average capacity C, we start from the received waveform during the nth frame

$$r_n(t) = \sqrt{\frac{\mathcal{E}_s(n_s)}{N_f}}\, s(n_s)\, h(t) + \eta_n(t),\ t \in [0, T_f) \tag{8}$$

for all $n \in [0, \bar{N}_s - 1]$, where $n_s := \lfloor n/N_f \rfloor$ takes the integer part of n/N_f and denotes the index of the information symbol $s(n_s)$ transmitted during the nth frame.

Using $\hat{h}(t)$ as a template, the correlator output is sampled at frame rate, and is given by

$$\begin{aligned} x(n) &= \int_0^{T_f} r_n(t)\hat{h}(t)dt \\ &= \int_0^{T_f}\left[\sqrt{\frac{\mathcal{E}_s(n_s)}{N_f}}s(n_s)h(t)+\eta_n(t)\right]\left[h(t)+\tilde{h}(t)\right]dt \\ &= \sqrt{\frac{\mathcal{E}_s(n_s)}{N_f}}\,\mathcal{E}_h\, s(n_s) + \zeta(n) \end{aligned} \tag{9}$$

where $\mathcal{E}_h := \int_0^{T_f} h^2(t)dt$ captures the gain provided by the channel, and $\zeta(n) := \zeta_1(n) + \zeta_2(n) + \zeta_3(n)$ is the filtered and sampled noise induced by AGN, expressed as the superposition of three terms

$$\begin{aligned} \zeta_1(n) &:= \int_0^{T_f} h(t)\eta_n(t)dt \\ \zeta_2(n) &:= \sqrt{\frac{\mathcal{E}_s(n_s)}{N_f}}s(n_s)\int_0^{T_f} h(t)\tilde{h}(t)dt \\ \zeta_3(n) &:= \int_0^{T_f}\tilde{h}(t)\eta_n(t)dt. \end{aligned}$$

We prove in Appendix I that the first two terms are zero-mean Gaussian random variables, whose autocorrelation functions are given by

$$\begin{aligned} E[\zeta_1(n)\zeta_1(n+k)|\{h(t)\}] &\approx \frac{\sigma^2}{2}\mathcal{E}_h\cdot\delta(k) \\ E[\zeta_2(n)\zeta_2(n+k)|\{h(t)\}] &\approx \frac{\sigma^2_{\hat{h}}}{2}\frac{\sqrt{\mathcal{E}_s(n_s)\mathcal{E}_s(k_s)}}{N_f}\mathcal{E}_h \end{aligned} \tag{10}$$

where $n_s := \lfloor n/N_f \rfloor$ and $k_s := \lfloor (n+k)/N_f \rfloor$ represent the symbol index corresponding to information-conveying frames n and $n+k$, respectively. Notice that $\zeta_1(n)$ is white, while $\zeta_2(n)$ is not. Moreover, we prove in Appendix I that $\zeta_3(n)$ is also approximately white Gaussian, with zero mean, and autocorrelation function

$$E[\zeta_3(n)\zeta_3(n+k)] \approx \frac{\sigma^2\sigma_{\hat{h}}^2}{2} BT_f \cdot \delta(k). \tag{11}$$

Recalling that each symbol is present in N_f frames, the decision statistic for the n_sth symbol $s(n_s)$ is formed by summing up N_f correlator output samples

$$y(n_s) = \sum_{n=n_sN_f}^{(n_s+1)N_f-1} x(n) = \sqrt{N_f \mathcal{E}_s(n_s)}\, \mathcal{E}_h\, s(n_s) + \xi(n_s)$$

where $\xi(n_s) := \sum_{n=n_sN_f}^{(n_s+1)N_f-1} \zeta(n)$ is zero mean Gaussian. In Appendix I, we establish that ζ_1, ζ_2, ζ_3 are approximately uncorrelated. Using this fact along with (10) and (11), we find that the variance of $\xi(n_s)$ is

$$\begin{aligned}\sigma_{\xi(n_s)}^2 &:= E[\xi^2(n_s)|\{h(t)\}] \\ &= \frac{N_f}{2}\mathcal{E}_h\sigma^2 + \frac{N_f}{2}\sigma_{\hat{h}}^2[\mathcal{E}_h\mathcal{E}_s(n_s) + BT_f\sigma^2] \end{aligned} \tag{12}$$

where to establish the second equality, we also used the fact that $\lfloor n/N_f \rfloor = \lfloor (n+k)/N_f \rfloor = n_s$, $\forall n, n+k \in [n_sN_f, (n_s+1)N_f)$. Consequently, the effective SNR for the n_sth received symbol is given by

$$\rho_{\text{eff}}(n_s) = \frac{2\mathcal{E}_h^2\mathcal{E}_s(n_s)}{\mathcal{E}_h\sigma^2 + [\mathcal{E}_h\mathcal{E}_s(n_s) + BT_f\sigma^2]\sigma_{\hat{h}}^2}. \tag{13}$$

Let us view our system in Fig. 1 from its binary input $s(n_s)$ to its binary output $\hat{s}(n_s)$. The probability that an input symbol $s(n_s)$ is erroneously decoded is determined by its corresponding effective SNR, $\rho_{\text{eff}}(n_s)$, and is given by

$$\begin{aligned} p(n_s) &:= P\{\hat{s}(n_s) = 1 | s(n_s) = -1\} \\ &= P\{\hat{s}(n_s) = -1 | s(n_s) = 1\} \\ &= Q\left(\sqrt{\rho_{\text{eff}}(n_s)}\right) \end{aligned} \tag{14}$$

where $Q(x) := (1/\sqrt{2\pi}) \int_x^\infty \exp(-y^2/2)dy$. Accordingly, the overall system, including the pulse shaper, the physical channel, the correlation receiver, and the symbol decoder, can be viewed as a binary symmetric channel (BSC) with transition probability $p(n_s)$, which varies from symbol to symbol. For such channels, the mutual information between $\hat{s}(n_s)$ and $s(n_s)$ is given by

$$\begin{aligned} &I(\hat{s}(n_s), h(t); s(n_s)) \\ &= E_{h,\hat{s},s}\left[\log_2 \frac{P\{\hat{s}(n_s), h(t) | s(n_s)\}}{P\{\hat{s}(n_s), h(t)\}}\right] \\ &= E_h\left[E_{\hat{s},s}\left[\log_2 \frac{P\{\hat{s}(n_s) | h(t), s(n_s)\}}{P\{\hat{s}(n_s) | h(t)\}}\right]\right] \end{aligned} \tag{15}$$

where the outer expectation is taken over the random channel's probability density function (pdf), i.e., the pdf of γ_l and τ_l; and the inner expectation, conditioned on each channel realization $h(t)$, is the mutual information for the BSC. For BSC, the mutual information is maximized when the input is symmetrically distributed: $P\{s(n_s) = 1\} = P\{s(n_s) = -1\} = 0.5$ (see, e.g., [11, Ch. 7]). Recalling the fact that for each transmitted burst, N_s out of N symbols are information-conveying, the resulting average capacity is given by

$$\begin{aligned} C = \frac{1}{N} \max_{P\{s(n_s)\}} \sum_{n_s=0}^{N_s-1} I(\hat{s}(n_s), h(t); s(n_s)) = \frac{1}{N} E_h \\ \cdot \left[\sum_{n_s=0}^{N_s-1} p(n_s)\log_2 p(n_s) + (1-p(n_s))\log_2(1-p(n_s)) + 1\right]. \end{aligned} \tag{16}$$

In the ensuing subsections, we will maximize this average capacity over our design parameters. Specifically, we will determine how to allocate energy between pilot and information waveforms, how to distribute energy among information symbols, and how many pilot waveforms to transmit per burst.

A. Optimizing Over Information Symbol Energy

The first step of our optimization is carried over the energy distribution among information symbols. Defining the "instantaneous" (per channel realization) capacity as

$$C_i := \sum_{n_s=0}^{N_s-1} p(n_s)\log_2 p(n_s) + (1-p(n_s))\log_2(1-p(n_s)) + 1$$

the average capacity in (16) is the averaged C_i/N over the channel pdf. To maximize C for any given burst size N, it suffices to maximize C_i for every channel realization. Maximizing C_i over the energy distribution among information symbols, we obtain the following result.

Proposition 2: For any given energies $\mathcal{E}_s$, $\mathcal{E}_p$, and burst size N, equi-powered information symbols maximize the instantaneous capacity C_i, and thus, the average capacity C.

Proof: See Appendix II. ■

Substituting $\mathcal{E}_s(n_s) := \mathcal{E}_s/N_s$ into (13), we have

$$\rho_{\text{eff}}(n_s) = \frac{2\mathcal{E}_h^2\mathcal{E}_s}{N_s\mathcal{E}_h\sigma^2 + (\mathcal{E}_h\mathcal{E}_s + N_sBT_f\sigma^2)\sigma_{\hat{h}}^2} =: \rho_{\text{eff}} \tag{17}$$

for all $n_s \in [0, N_s - 1]$. The average capacity in (16) is now given by

$$C = \frac{N_s}{N} E[p\log_2 p + (1-p)\log_2(1-p) + 1] \tag{18}$$

where the transition probability $p := Q\left(\sqrt{\rho_{\text{eff}}}\right)$ is now the same for all $n_s \in [0, N_s - 1]$. It is worth stressing that the number of waveforms per information symbol N_f is an important parameter in UWB transmissions. Although it does not explicitly appear in (17), N_f affects ρ_{eff} and C by altering N_s for any fixed N and energy allocation.

When the channel estimate is perfect, i.e., $\hat{h}(t) = h(t)$, the only noise term left is $\zeta_1(n)$, and the effective SNR becomes

$$\rho_{\text{eff}} = \frac{2\mathcal{E}_s\mathcal{E}_h}{N_s\sigma^2} \tag{19}$$

which provides an upper bound on the effective SNR when channel estimation errors are present. Its corresponding C, de-

noted with $\bar{C}$, gives an upper bound on the average capacity associated with imperfect channel estimates.

B. Linking Capacity With Channel MSE

So far, we have established that equi-powered information waveforms are optimal in the sense of maximizing average capacity for any given information energy $\mathcal{E}_s$. Recall also that in the previous section, we showed that equi-powered pilot waveforms minimize the channel MSE for any given pilot energy $\mathcal{E}_p$. Channel MSE affects the overall system performance, while (16) provides a measure of achievable information rate of the underlying system. How optimal are the equi-powered waveforms in the sense of maximizing C?

We will show next that maximizing C is equivalent to minimizing $\sigma^2_{\hat{h}}$. Differentiating C with respect to ρ_{eff}, and treating N and N_s as constants, we have

$$\frac{\partial C}{\partial \rho_{\text{eff}}} = \frac{N_s}{N2\sqrt{2\pi}} E\left[\frac{1}{\sqrt{\rho_{\text{eff}}}} \exp\left(-\frac{\rho_{\text{eff}}}{2}\right) \log_2 \frac{1-p}{p}\right] > 0 \quad (20)$$

because $1 - p > 0.5 > p$, $\forall \rho_{\text{eff}}$. Furthermore, ρ_{eff} increases monotonically with decreasing $\sigma^2_{\hat{h}}$ [cf. (17)] for fixed $\mathcal{E}_s$, $\mathcal{E}_p$, and σ^2. Therefore, the equi-powered pilot waveforms (cf. Proposition 1) not only minimize channel MSE, but also maximize the average capacity.

C. Optimizing Over the Number of Pilot Waveforms

As is evident from (18), increasing N_s boosts C for any given burst size N. Although not as evident, C also depends on N_s through p, which in turn depends on ρ_{eff}. Referring to (17), we observe that with other parameters fixed, ρ_{eff} decreases as N_s increases. The resulting increase in p causes C to decrease. In short, increasing the number of pilot waveforms $\bar{N}_p$ enhances C through increasing ρ_{eff}, but reduces C through decreasing N_s/N.

To find out the optimal $\bar{N}_p$, and thus, N_s, that results in the maximum C, we first show that:

Lemma 1: For any given information energy $\mathcal{E}_s$, pilot energy $\mathcal{E}_p$, and number of waveforms per burst $\bar{N}$, the average capacity C decreases monotonically as the number of pilot waveforms $\bar{N}_p$ increases beyond $\bar{N}^*_p := (N - N^*_s)N_f$, where N^*_s is given by

$$N^*_s = \begin{cases} \frac{\bar{N}}{N_f} - 1, & \text{if } \frac{\bar{N}}{N_f} \text{ is an integer} \\ \left\lfloor \frac{\bar{N}}{N_f} \right\rfloor, & \text{otherwise.} \end{cases} \quad (21)$$

Proof: As described in Section II, each burst contains $\bar{N}$ waveforms. Each of the waveforms is used either as a pilot waveform, or, as an information-bearing waveform through binary modulation. In terms of the number of pilot waveforms $\bar{N}_p$, the number of information symbols is given by

$$N_s = \frac{\bar{N}_s}{N_f} = \left\lfloor \frac{\bar{N} - \bar{N}_p}{N_f} \right\rfloor \quad (22)$$

since each symbol is transmitted via N_f waveforms. It follows that the maximum number of information symbols in a burst containing $\bar{N}$ waveforms is given by (21). Notice that when N is an integer, N_f waveforms are reserved as pilots. Consequently, the minimum number of pilot waveforms in a size N burst is given by $\bar{N}^*_p = (N - N^*_s)N_f$.

For any given energies $\mathcal{E}_p$, $\mathcal{E}_s$, and $\bar{N}$, if we keep $N_s \leq N^*_s$ fixed, then varying $\bar{N}_p$ in the range $[\bar{N}^*_p, \bar{N} - \bar{N}_s]$ does not affect ρ_{eff} in (17). Consequently, C also stays unaffected as $\bar{N}_p$ varies within this range. Therefore, finding the optimal $\bar{N}_p$ is equivalent to finding the optimal $N_s \leq N^*_s$ while fixing $\bar{N}_p = \bar{N}^*_p$. In other words, given a total energy $\mathcal{E}_s$ and a block length N^*_s, we have to select $N_s \leq N^*_s$, and distribute the total energy uniformly in order to maximize C. As stated in Proposition 2 and proved in Appendix II, with any fixed total energy and block length, equi-powered information symbols maximize C. Consequently, we should choose $N_s = N^*_s$, and $\bar{N}_p = \bar{N}^*_p$. As $\bar{N}_p$ increases beyond $\bar{N}^*_p$, the average capacity will decrease. ■

Over each burst containing $\bar{N}$ waveforms, Lemma 1 asserts that we should use $\bar{N}^*_s := N^*_s N_f$ as information-bearing waveforms, and concentrate the available energy for training $\mathcal{E}_p$ to the rest $\bar{N}^*_p \leq N_f$ pilot waveforms. As a consequence of Lemma 1, the optimal number of pilot waveforms is chosen according to the following proposition.

Proposition 3: For any given information energy $\mathcal{E}_s$, pilot energy $\mathcal{E}_p$, and number of waveforms per burst $\bar{N}$, the number of pilot waveforms $\bar{N}_p$ that maximizes the average capacity C is given by $\bar{N}^*_p$, which is defined in Lemma 1.

The number of waveforms per burst $\bar{N}$ is determined by the channel coherence time τ_c. Notice that for any $\bar{N}$ and total energy $\mathcal{E}$, the optimal number of pilot waveforms is no more than N_f. Theoretically, we could always choose $\bar{N} \leq \lfloor \tau_c/T_f \rfloor$ such that $\bar{N} = N^*_s N_f + 1$, where $N^*_s = \lfloor \bar{N}/N_f \rfloor$ [cf. (21)]. In other words, the optimal number of pilot waveforms is always $\bar{N}^*_p = 1$. However, such a choice results in maximum peak-to-average power ratio for a fixed pilot energy $\mathcal{E}_p$, and is also prone to timing offset. Therefore, it is more desirable to choose $\bar{N} = \lfloor \tau_c/T_f \rfloor$, and determine $\bar{N}^*_p$ according to Proposition 3. When $\bar{N}_p = \bar{N}^*_p$, the maximum average capacity is given by

$$C = \frac{N^*_s}{N} E[p \log_2 p + (1-p)\log_2(1-p) + 1] \quad (23)$$

where the effective SNR that p depends on is

$$\rho_{\text{eff}} = \frac{2\mathcal{E}^2_{\hat{h}} \mathcal{E}_s}{N^*_s \mathcal{E}_h \sigma^2 + (\mathcal{E}_h \mathcal{E}_s + N^*_s B T_f \sigma^2)\sigma^2_{\hat{h}}}. \quad (24)$$

To complete our optimal PWAM design, we need to determine how to allocate the total transmission energy per burst $\mathcal{E}$ to information and pilot waveforms.

D. Optimizing Over the Energy Allocation

As shown earlier [see (20)], for fixed N and N_s, maximizing C is equivalent to maximizing ρ_{eff} in (17). From (7), we observe that as $\mathcal{E}_p$ increases, $\sigma^2_{\hat{h}}$ decreases and tends to enhance ρ_{eff}. But at the same time, $\mathcal{E}_s$ also decreases and tends to reduce ρ_{eff}. The maximization then amounts to optimally allocating the fixed transmission energy per burst $\mathcal{E}$ among information and pilot waveforms.

Defining the energy allocation factor $\alpha := \mathcal{E}_s/\mathcal{E} \in (0, 1)$ as the fraction of the total transmission energy per burst that is

allocated to information waveforms, we have, accordingly, $\mathcal{E}_p = (1-\alpha)\mathcal{E}$. Also defining $\rho := \mathcal{E}/(N\sigma^2)$ as the nominal SNR per received symbol, we can rewrite (17) into a more convenient form

$$\rho_{\text{eff}} = \frac{2\alpha(1-\alpha)\mathcal{E}_h^2 N^2\rho^2}{[\alpha + N_s(1-\alpha)]\mathcal{E}_h N\rho + N_s BT_f}. \tag{25}$$

Differentiating ρ_{eff} with respect to α for each of the following cases, we have:

1) When $N_s = 1$, (25) becomes

$$\rho_{\text{eff}} = \frac{2\alpha(1-\alpha)\mathcal{E}_h^2 N^2\rho^2}{\mathcal{E}_h N\rho + BT_f}. \tag{26}$$

As a result, $\alpha = 1/2$ yields the maximum effective SNR

$$\rho_{\text{eff}} = \frac{\mathcal{E}_h^2 N^2\rho^2}{2(\mathcal{E}_h N\rho + BT_f)}. \tag{27}$$

2) When $N_s > 1$, it turns out that

$$\alpha = \frac{N_s(\mathcal{E}_h N\rho + BT_f)}{\mathcal{E}_h N\rho(N_s-1)}\left(1 - \sqrt{1 - \frac{\mathcal{E}_h N\rho(N_s-1)}{N_s(\mathcal{E}_h N\rho + BT_f)}}\right) \tag{28}$$

maximizes ρ_{eff}. The optimal energy allocation factor in (28) can be further simplified as follows:

a) At low SNR ($N\rho \ll BT_f$), using the approximation $\sqrt{1-\epsilon} \approx 1 - \epsilon/2, \forall \epsilon \ll 1$, we have

$$\alpha = \frac{1}{2}$$
$$\text{and} \quad \rho_{\text{eff}} = \frac{\mathcal{E}_h^2 N^2\rho^2}{(N_s+1)\mathcal{E}_h N\rho + 2N_s BT_f}. \tag{29}$$

b) If $N\rho \gg BT_f$, we have

$$\alpha = \frac{\sqrt{N_s}}{\sqrt{N_s}+1}$$
$$\text{and} \quad \rho_{\text{eff}} = \frac{2\mathcal{E}_h^2 N^2\rho^2}{(\sqrt{N_s}+1)^2(\mathcal{E}_h N\rho + \sqrt{N_s}T_f)}. \tag{30}$$

Notice that (30) is valid not only with high SNR ($\rho \gg$), but also with moderate SNR when burst size is sufficiently large ($N \gg$). The latter is oftentimes the case since UWB is generally employed for indoor environments with low-to-moderate mobility. Also notice that (29) and (30) provide us with general expressions $\forall N_s \geq 1$, since they boil down to (27) when $N_s = 1$. We can now summarize our results in the following proposition.

Proposition 4: With fixed burst size N, number of information symbols per burst N_s, and total transmission energy per burst $\mathcal{E}$, the optimal energy allocation factor $\alpha = \mathcal{E}_s/\mathcal{E}$ that maximizes C is given by

$$\begin{cases} \alpha = \frac{1}{2}, & \text{for } N\rho \ll BT_f \\ \alpha = \frac{\sqrt{N_s}}{\sqrt{N_s}+1}, & \text{for } N\rho \gg BT_f. \end{cases} \tag{31}$$

The optimization over the energy allocation factor α is carried out for any given total transmission energy $\mathcal{E}$, burst size N, and number of information symbols per burst N_s. Therefore, this optimization step does not affect any of the preceding optimal parameter designs. In fact, all of the preceding optimization steps are decoupled. Consequently, they provide together an overall optimal PWAM design.

V. Extensions and Discussion

In Sections III and IV, we successfully designed an optimal PWAM. The design minimizes channel estimation MSE, and maximizes the average capacity of the overall system simultaneously. The optimal PWAM parameters are given in Propositions 1–4, and will be verified by simulations in Section VI. Nevertheless, besides the channel MMSE and average capacity, there might be other concerns when implementing power-limited UWB communication systems. In this section, we will modify our optimal PWAM to fit some of these concerns.

A. $\bar{N}_p$ as an Integer Multiple of N_f

To transmit one information symbol in UWB transmissions, the monocycle waveform is repeated over N_f frames. To be realized with low complexity, our optimal PWAM can be modified so that pilot waveforms are also transmitted in groups of size N_f.

It is evident that under such a constraint, Propositions 1 and 2 still hold true without modification. According to Proposition 3, in order to have $\bar{N}_p^* = N_f$, the number of waveforms per burst should be chosen as $\bar{N} = \lfloor \tau_c/(N_f T_f) \rfloor N_f$. Treating N_f pilot waveforms as one pilot symbol-waveform, we find the optimal number of pilot symbol-waveforms $N_p = 1$. Since $\bar{N}_p$ is still the smallest possible in this case, C is maximized over all possible $\bar{N}_p$'s that are integer multiples of N_f. Taking into account that $N_s^* = N - 1, \forall N$, the optimal energy allocation factor is given by

$$\begin{cases} \alpha = \frac{1}{2}, & \text{for } N\rho \ll BT_f \\ \alpha = \frac{\sqrt{N-1}}{\sqrt{N-1}+1}, & \text{for } N\rho \gg BT_f. \end{cases} \tag{32}$$

Similar to the definition of nominal SNR ρ, we define the information SNR and the pilot SNR in terms of ρ as follows:

$$\text{information SNR}: \rho_s := \frac{\mathcal{E}_s}{N_s\sigma^2} = \frac{N}{N_s}\alpha\rho$$
$$\text{pilot SNR}: \rho_p := \frac{\mathcal{E}_p}{N_p\sigma^2} = \frac{N}{N_p}(1-\alpha)\rho. \tag{33}$$

We observe that generally $\rho_s \neq \rho_p$.

B. Equi-SNR Pilots and Information Symbols

The discrepancy between ρ_s and ρ_p results in uneven instantaneous transmit-power levels, which challenges the power amplification stage. To avoid such problems, the same information and pilot SNR $\rho_s = \rho_p$ may be desirable in order to maintain a transmission where all monocycle pulses have the same amplitude. It follows from (33) that

$$\frac{\alpha}{N_s} = \frac{1-\alpha}{N_p} = \frac{1-\alpha}{N-N_s} \Leftrightarrow \alpha = \frac{N_s}{N},\ 1-\alpha = \frac{N_p}{N} \tag{34}$$

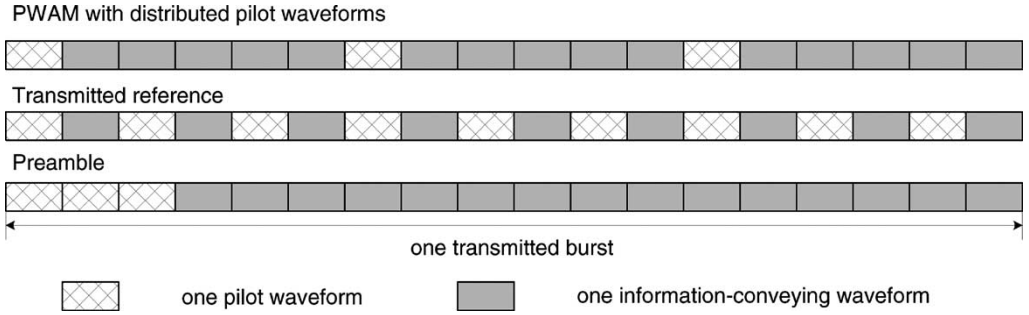

Fig. 2. Placement of pilot waveforms for PWAM, TR, and preamble ($N_f = 3$, $\bar{N}_p = 3$, $\bar{N} = 18$).

is required. Substituting (34) into (25), we have the effective SNR given by

$$\rho_{\text{eff}} = \frac{2(1-\alpha)N\mathcal{E}_h^2\rho^2}{(1-\alpha)N\mathcal{E}_h\rho + \mathcal{E}_h\rho + BT_f} \tag{35}$$

and the average capacity given by [cf. (18)]

$$C = \alpha E[p\log_2 p + (1-p)\log_2(1-p) + 1]. \tag{36}$$

Once again, we observe the opposing trends of C as N_p increases. But this time, the energies $\mathcal{E}_s$ and $\mathcal{E}_p$ not only change with N_p, but are also uniquely determined by N_p for a fixed burst size N. Therefore, this optimization problem differs from the one in the previous section, where the optimization of $\mathcal{E}_s$ and N_p can be decoupled and carried out independently, to reach a globally optimum solution. In this case, we will resort to numerical search to find this optimal N_p subject to $\rho_s = \rho_p$. The resulting PWAM maximizes C under the aforementioned equi-SNR constraint, and we abbreviate it as optimal ES-PWAM. When $N = 2$, the only choice is $N_s = N_p = 1$, and $\alpha = 0.5$. This choice coincides with our optimal PWAM design.

C. PWAM With PPM

If binary PPM is employed in lieu of binary PAM, the analysis will be more complicated, but can still be carried out in the same manner with some modifications. In our analysis based on binary PAM, the correlator template is just the channel estimate $\hat{h}(t)$. The sign of the correlator output then determines the decoded symbol (± 1). When PPM is used, $+1$ is represented by the pulse $w(t)$, while -1 is represented by the delayed pulse $w(t-\Delta)$, with $\Delta > 0$. The resulting modulation becomes orthogonal when Δ is sufficiently large so that the correlation between the two pulses is zero. For both orthogonal and nonorthogonal PPM, if we use $\hat{h}(t) - \hat{h}(t-\Delta)$ as the correlator template, then the decoded symbol can still be determined by the sign of the correlator output, as with PAM (see, e.g., [14]). The rest of the analysis can, thus, be carried out as presented in this paper.

D. Performance-Rate Tradeoff

As we mentioned in the introduction, the recently proposed TR transmission for UWB communications shares some features with our PWAM design. They both average previously received pilot waveforms (so-called TR in [3] and [6]) to form the correlator template at the receiver. The difference is that PWAM optimally trades off channel estimation performance for information rate, while TR always utilizes half of the transmitted waveforms as pilots [3], [6]. Interestingly, when $N = 2$, we have $N_p = N_s = 1$, and $\alpha = 1/2$ for optimal PWAM. In this case only, half of the equi-powered transmitted waveforms are used as pilots. The resulting PWAM-UWB system turns out to be equivalent to the TR signalling scheme, which reveals the optimality of TR in this special case. In fact, in optimal PWAM, the number of pilots satisfies $N_s \geq N/2$, and is, thus, always no less than that in TR. Moreover, ρ_{eff} is maximized in optimal PWAM for any N_s, and is also always no less than that in TR. The equality only occurs when $N = 2$. As a result, TR is not optimal for $N \neq 2$, but is optimal when $N = 2$. As a matter of fact, the flexibility inherent to PWAM allows it to span the gamut of performance-critical to rate-critical scenarios. When the channel does not vary much over time, a large τ_c allows for a large burst size N, and PWAM increases information rate by using a small number of pilot waveforms. The placement of pilot waveforms for all PWAM, TR, and preamble schemes is shown in Fig. 2. Notice that while preamble training enjoys similar bandwidth efficiency, PWAM is more immune to slow channel variation by distributing pilot waveforms throughout each burst. On the other extreme, when the channel varies rapidly, PWAM trades in information rate for improved channel estimation performance by adapting the number of pilot waveforms to the channel coherence time. To this effect, TR is also robust to channel variations, but may unnecessarily sacrifice information rate when the channel does not vary over a group of symbols.

VI. Simulations

In this section, we present simulations and comparisons to validate our analyses and designs. In all cases, the random channels are generated according to [8] and [13], where rays arrive in several clusters within an observation window. The cluster arrival times are modeled as Poisson variables with cluster arrival rate Λ. Rays within each cluster also arrive according to a Poisson process with ray arrival rate λ. The amplitude of each arriving ray is a Rayleigh distributed random variable having exponentially decaying mean square value with parameters Γ and γ. Parameters of this channel model are chosen as $\Gamma = 30$ ns, $\gamma = 5$ ns, $1/\Lambda = 2$ ns, and $1/\lambda = 0.5$ ns. The diminishing tail of the multipath channel power profile is cut off to make the maximum delay spread of the multipath channel $T_g = 98$ ns. We select the pulse shaper as the second derivative

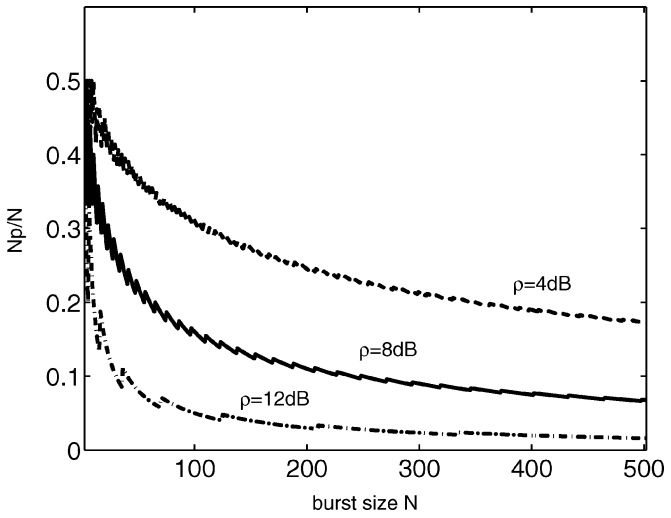

Fig. 3. ES-PWAM: Optimal number of pilots N_p versus burst size N, at three nominal SNR levels $\rho = 4, 8, 12$ dB.

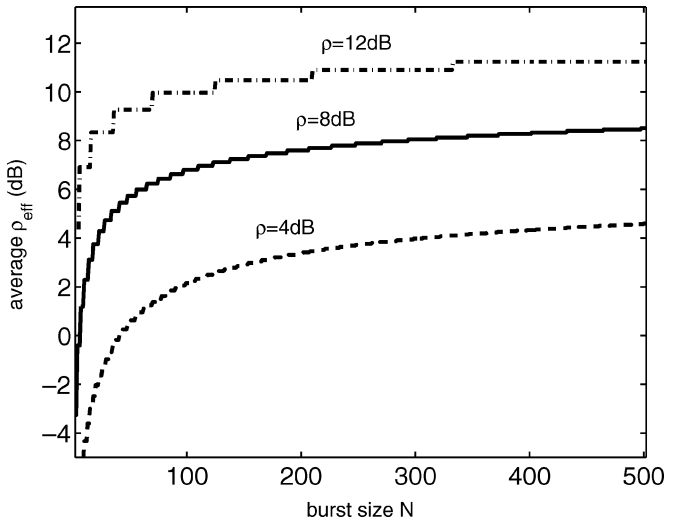

Fig. 4. ES-PWAM: Average effective SNR ρ_{eff} associated with optimal number of pilots N_p versus burst size N, at three nominal SNR levels $\rho = 4, 8, 12$ dB.

of the Gaussian function $\sqrt{\tau^3/3}(2/\pi)^{1/4}\exp(-t^2/\tau^2)$, which has been normalized to have unit energy. The parameter τ is chosen to be 0.32 ns to obtain a pulsewidth of approximately 2.0 ns. The frame duration is chosen to be $T_f = 100$ ns [20]. The receiver front end is modeled as an ideal bandpass filter with center frequency $f_0 = 1.1$ GHz and double-sided bandwidth of $B = 1.6$ GHz, which corresponds to the -15-dB bandwidth of the monocycle $w(t)$. For ease of comparisons, the optimal PWAM is designed with integer N_p's, unless otherwise specified.

A. Test A: [Optimal ES-PWAM]

To carry out comparisons, we will first find the optimal number of pilots N_p of our ES-PWAM associated with variable burst size N, and nominal SNR ρ.

Case 1 (burst size N): As the burst size N increases, we observe from Fig. 3 that the optimal ratio N_p/N decreases as N increases, which reveals the fact that as burst size increases, a smaller percentage of waveforms are used as pilot waveforms. The average effective SNR ρ_{eff} [cf. (35)] associated with the optimal number of pilots N_p is also plotted in Fig. 4.

Case 2 (nominal SNR ρ): For five different burst sizes, Fig. 5 shows that as SNR increases, N_p decreases. As a matter of fact, a single pilot symbol ($N_p = 1$) per burst is needed when the nominal SNR exceeds 17 dB.

B. Test B: [Average Capacity]

In this example, we compare the average capacity of our optimal PWAM with the ES-PWAM, and with the TR signalling scheme [3].

Case 1 (number of pilots N_p): In this case, the behavior of C is studied as N_p increases with fixed burst size N. Two energy allocation schemes are used: One is the optimal energy allocation with α that varies with N_p; and the other is an arbitrarily chosen $\alpha = 0.8$ that is fixed as N_p changes. Fig. 6 shows that the average capacity associated with both allocation schemes decreases monotonically as N_p increases, while the optimal α always outgoes $\alpha = 0.8$, as we expected.

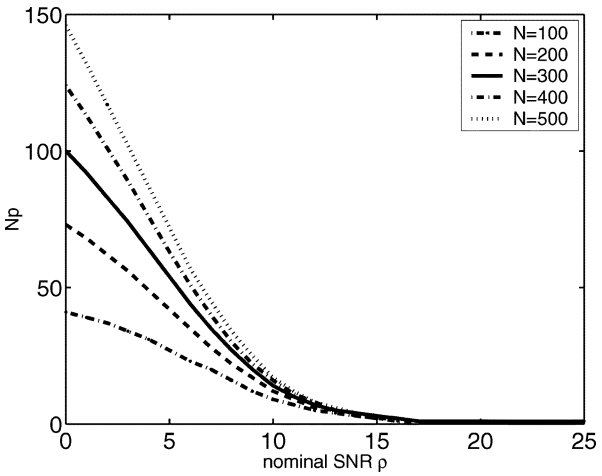

Fig. 5. ES-PWAM: Optimal ratio of N_p versus nominal SNR ρ, for burst sizes $N = (100, 200, 300, 400, 500)$.

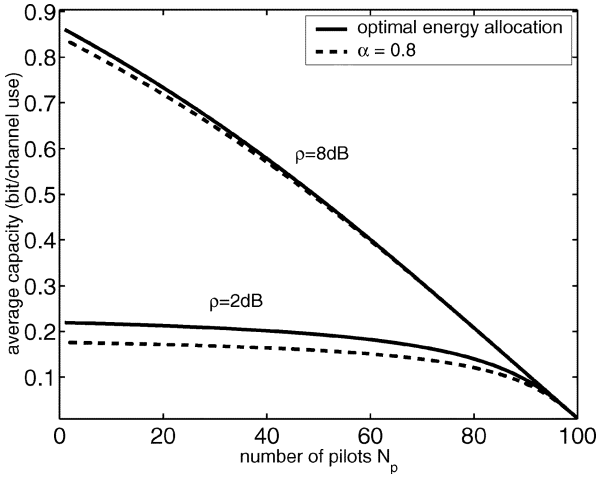

Fig. 6. Average capacity versus number of pilots (burst size $N = 100$).

Case 2 (burst size N): For various burst sizes, Fig. 7 depicts the average capacity associated with an ideal channel estimate,

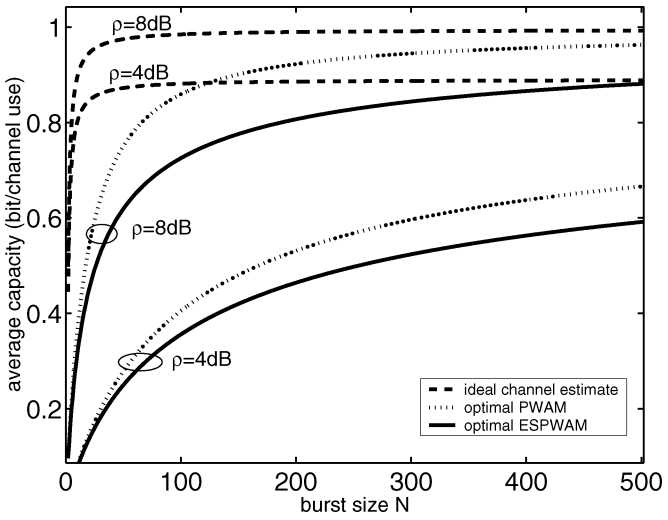

Fig. 7. Average capacity versus burst size N.

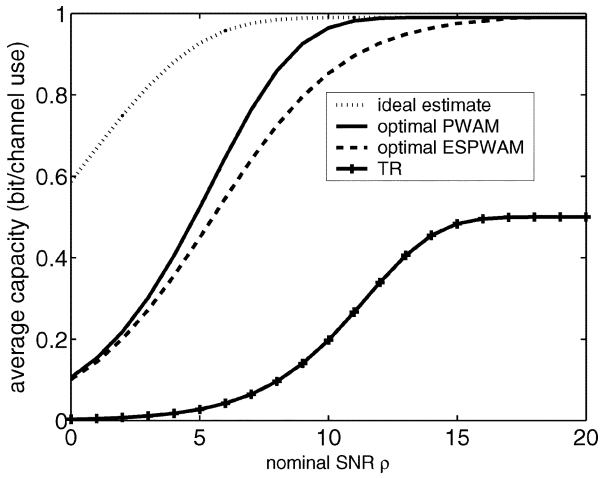

Fig. 8. Average capacity versus nominal SNR ρ (burst size $N = 100$).

optimal PWAM, and optimal ES-PWAM. For both SNR levels, the optimal PWAM outperforms ES-PWAM. This is due to the fact that ES-PWAM has smaller N_s and smaller ρ_{eff}, in comparison with PWAM. Consequently, ES-PWAM can only yield a suboptimal C.

Case 3: (nominal SNR ρ): Fig. 8 depicts not only the C associated with our optimal (ES)PWAM, but also the C associated with TR [3]. The gap is evident, and is increasing as SNR increases. Notice that at high SNR, C corresponding to PWAM approaches one, whereas, that corresponding to TR approaches 0.5 due to its inherent 50% rate loss.

C. Test C: [BER Performance]

The average capacity provides us with a comprehensive means of measuring both performance and information rate, while our optimal PWAM provides optimal tradeoffs between them. To explicitly observe these tradeoffs, we carry out further performance comparisons.

Case 1 (optimal versus ideal): With a channel coherence time of 1 ms, each burst contains $\bar{N} = 10\,000$ waveforms. The average bit-error rate (BER) versus the ratio $\mathcal{E}/\sigma^2$ is plotted in Fig. 9, for $N_f = (20\,100)$. The gap observed relative to the ideal

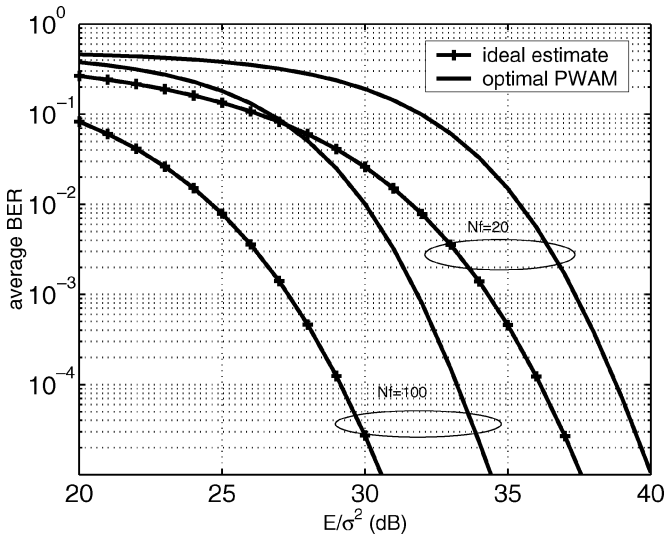

Fig. 9. BER performance of optimal PWAM. Each burst of duration 1 ms (channel coherent time) contains $\bar{N} = 10\,000$ waveforms.

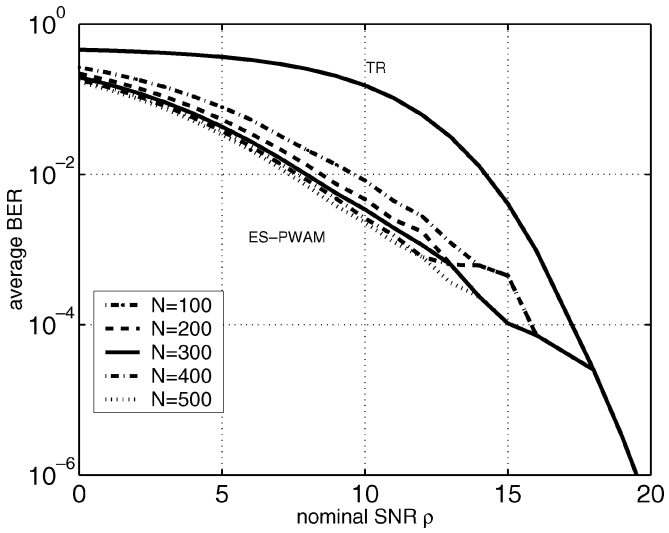

Fig. 10. BER performance comparison between ES-PWAM and TR with the same nominal SNR.

case (perfect channel knowledge) is due to the fact that PWAM, as well as TR [3], rely on a noisy template at the correlation receiver. As N_f increases, the BER performance of both our optimal PWAM and that of the ideal channel estimate improves, and their gap increases. The information rates associated with $N_f = (20\,100)$ are 499 and 99 Kb/s, respectively.

Case 2 (ES-PWAM versus TR): In the TR signalling scheme, pilot waveforms and information waveforms have the same SNR, i.e., $\rho_s = \rho_p$. To be fair, we compare TR with our optimal ES-PWAM. With channel coherence time of $\tau_c = (0.2, 0.4, 0.6, 0.8, 1.0)$ ms, we have $\bar{N} = (2, 4, 6, 8, 10) \times 10^3$ waveforms per burst. With $N_f = 20$ frames per symbol, we have burst sizes $N = (1, 2, 3, 4, 5) \times 10^2$. By dynamically adjusting the number of pilot waveforms per burst according to channel coherence time, as well as SNR, ES-PWAM outperforms TR for $\rho < 18$ dB, as depicted in Fig. 10. Notice that BER performance of ES-PWAM and TR converges after $\rho = 18$ dB. This is because TR averages

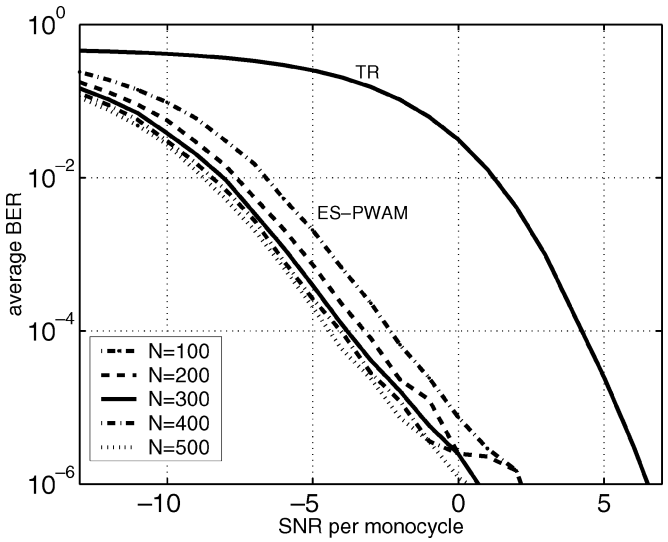

Fig. 11. BER performance comparison between ES-PWAM and TR with the same information rate.

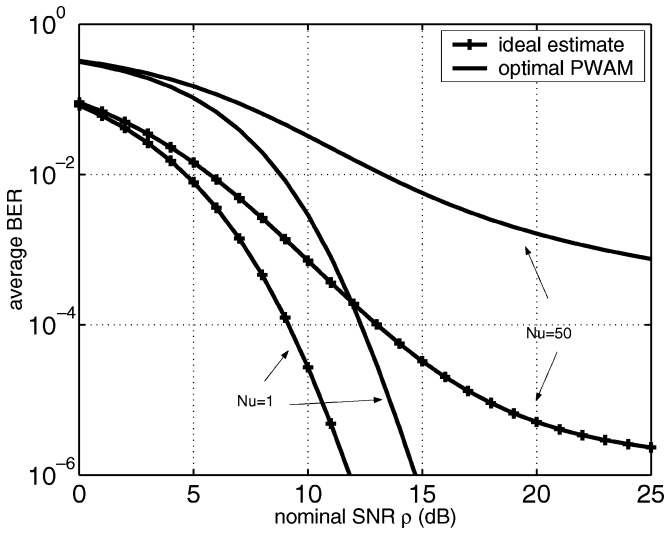

Fig. 12. BER performance of optimal PWAM in the presence of MUI ($N = 100$, $N_f = 20$).

over only one pilot symbol to obtain $\hat{h}(t)$ [3], regardless of coherence time and SNR; and ES-PWAM also uses a single pilot symbol after $\rho = 18$ dB [cf. Fig. 8]. Although their high-SNR performance is identical, the discrepancy of their rates is large. The information rate of TR is 250 Kb/s, whereas, that of ES-PWAM is 495 Kb/s with $\tau_c = 0.2$ ms and 499 Kb/s with $\tau_c = 1.0$ ms, respectively. To equate the rate, one can simply adjust N_f according to the channel coherence time. For the same information rate (250 Kb/s), the improved BER performance of ES-PWAM over TR is evidenced in Fig. 11.

D. Test D: [Robustness Issues]

Our analysis is carried out for a single-user link over a quasi-static multipath channel. When multiple users present, the multiuser problem can be rendered equivalent to a set of single user problems with appropriate user-specific spreading codes [21], where our analysis is directly applicable. Even when conventional time hopping (TH) is used, our PWAM is still applicable, treating multiuser interference (MUI) as noise. In the following, we will carry out simulations to test the robustness of our PWAM in the presence of MUI, timing offset, and channel variation.

Case 1 (in the presence of MUI): With channel coherence time $\tau_c = 0.2$ ms, and $N_f = 20$, the burst size is $N = 100$. Average BER versus nominal SNR ρ is plotted in Fig. 12 for both optimal PWAM and ideal channel estimate. Random TH code is used, and the MUI is modeled as Gaussian noise [20]. As multiple users are present, degradation in BER performance can be observed both with PWAM and with perfect channel estimate.

Case 2 (In the presence of timing offset): Imperfect timing will induce erroneous channel estimates, and will thereby affect BER performance. With coarse timing acquired using methods detailed in [17] and [22], we simulate the effect of the residual timing offset. The residual timing offset is modeled as either uniformly distributed within $[0, T_f)$, or exponentially distributed with mean 20 ns. Two values of channel coherence time are considered, with fixed $N_f = 50$. For $\tau_c = 25.1$ μs, we have $N_s = 5$ and $\bar{N}_p = 1$; while for $\tau_c = 27.5$ μs, we use $N_s = 5$ and $\bar{N}_p = 25$. As shown in Fig.13, the BER performance degradation induced by timing offset is significant when a single pilot waveform is used, but negligible when 25 pilot waveforms are averaged. Moreover, the uniformly distributed timing offset seems to be more harmful than the exponentially distributed one.

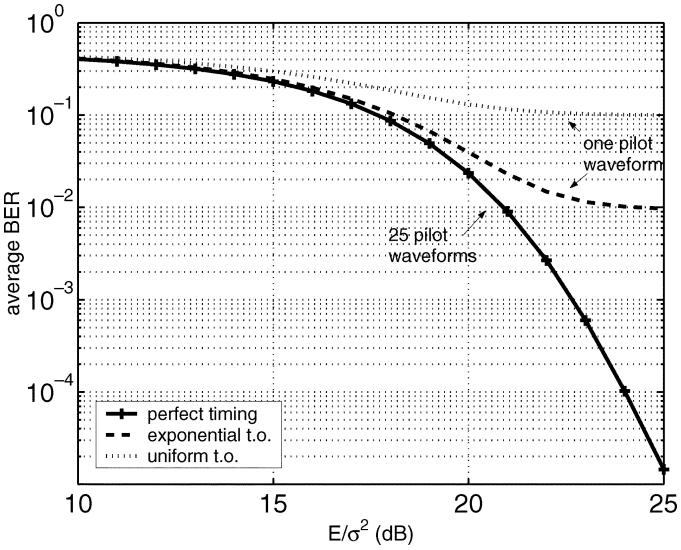

Fig. 13. BER performance of optimal PWAM in the presence of timing offset.

Case 3 (in the presence of channel variation): Although PWAM is established using the quasi-static multipath channel model, its flexibility in distributing the pilot waveforms provides robustness against slow channel variations. The channel MSE values of optimal PWAM and preamble training are compared in Fig. 14 over slowly time-varying multipath channels, at $\mathcal{E}_p/\sigma^2 = 15$ dB. The channel evolution per tap is generated using a first-order auto-regressive model $\gamma_l(t+\delta t) = 0.99e^{j\omega\delta t}\gamma_l(t) + v(t+\delta t)$, where $v(t)$ is white Gaussian with zero mean and standard deviation $5e-3$, and $\omega = (104, 243, 347)\pi$ rad/s for Channels A, B, and C, respectively. The channel MSE is plotted over five bursts

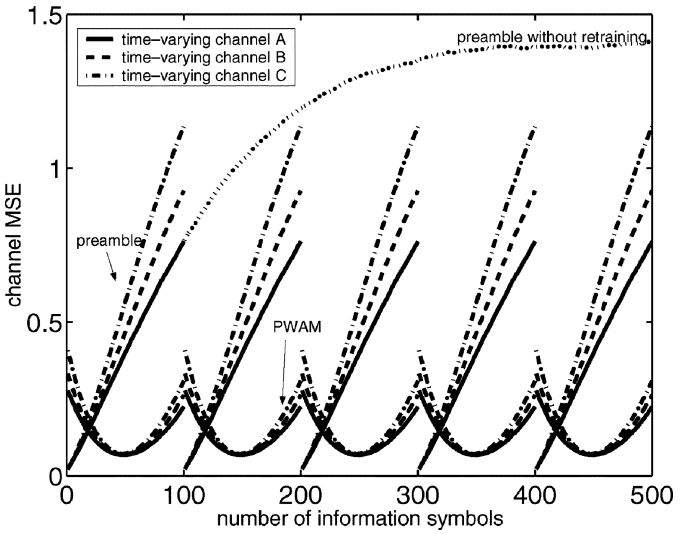

Fig. 14. Channel estimation performance of optimal PWAM and preamble training, in the presence of channel variation ($N = 101$, $N_f = 100$).

each containing $N_s = 100$ information symbols. To equate energy and information rates of the two schemes, the preamble method uses one pilot symbol at the very beginning of each burst, whereas, PWAM evenly distributes the $\bar{N}_p = 100$ pilot waveforms throughout each burst. Notice that at the beginning of each burst, the preamble method performs better since all pilot waveforms are gathered there. Nevertheless, channel MSE of the preamble method increases rapidly, and exceeds that of PWAM for about 80% information symbols out of each burst. Without periodic retraining, the preamble approach yields a consistently increasing channel MSE, as depicted by the dotted line in Fig. 14.

VII. Conclusion

In this paper, we have introduced a novel PWAM for UWB transmissions. We designed our PWAM parameters by optimizing both channel estimation performance and information rate. The resulting optimal PWAM minimizes channel MSE, and maximizes the average capacity of the underlying system. Our optimal PWAM is tailored for UWB communications, it relies only on frame rate samples, and can be applied to both PAM and PPM signalling. Simulation results confirmed the flexibility provided by PWAM in striking desirable performance-rate tradeoffs, and its robustness in the presence of MUI, timing offsets, and channel variations.

Appendix I
Noise Autocorrelation Functions

Let us first consider the sampled noise $\zeta_1(n)$. By definition, its autocorrelation function conditioned on $h(t)$ is given by (37), shown at the bottom of the page, where $H(f)$ is the Fourier transform of $h(t)$. Because the support of $h(t)$ is the frame duration T_f, the bandwidth of $H(f)$ is approximately $1/T_f$. Recalling that the bandwidth of the bandpass frontend $B \gg 1/T_f$, we deduce that the sum in the last equality of (37) boils down to $\int_{-\infty}^{+\infty} H(f)e^{j2\pi f(t-kT_f)}df \approx h(t-kT_f)$, and thus

$$E[\zeta_1(n)\zeta_1(n+k)|\{h(t)\}] \approx \frac{\sigma^2}{2}\int_0^{T_f} h(t)h(t-kT_f)dt = \frac{\sigma^2}{2}\mathcal{E}_h\delta(k) \quad (38)$$

where by definition, the Kronecker delta function is $\delta(k) = 1$ for $k = 0$, and 0 for $k \neq 0$. In other words, the sampled noise $\zeta_1(n)$ is white Gaussian with zero mean, and variance $\mathcal{E}_h\sigma^2/2$.

The second noise term $\zeta_2(n)$ contains channel estimation errors. Recalling that the same channel estimate $\hat{h}(t)$ is used throughout one burst, its autocorrelation function is given by

$$E[\zeta_2(n)\zeta_2(n+k)|\{h(t)\}] = \frac{\sqrt{\mathcal{E}_s(n_s)\mathcal{E}_s(k_s)}}{N_f} \times \int_0^{T_f}\int_0^{T_f} h(t)h(\tau)E[\tilde{h}(t)\tilde{h}(\tau)]d\tau dt \quad (39)$$

where $n_s := \lfloor n/N_f \rfloor, k_s := \lfloor (n+k)/N_f \rfloor$ represent the symbol index corresponding to information-conveying frames n and $n+k$, respectively. Substituting (5) into (39), we have

$$E[\zeta_2(n)\zeta_2(n+k)|\{h(t)\}] = \frac{\sigma_{\hat{h}}^2}{2}\frac{\sqrt{\mathcal{E}_s(n_s)\mathcal{E}_s(k_s)}}{N_f}\mathcal{E}_h. \quad (40)$$

Notice that $\tilde{h}(t)$ in $\zeta_2(n)$ and $\zeta_3(n)$ depends on $\eta_{n_p}(t)$ [cf. (3)], where n_p and n stand for pilot- and information-waveform indexes, respectively. Since pilot and information waveforms do not overlap in time, and $B \gg 1/T_f$, it follows that $\eta_{n_p}(t)$ is only weakly correlated with its adjacent $\eta_n(t)$. Con-

$$\begin{aligned}
E[\zeta_1(n)\zeta_1(n+k)|\{h(t)\}] &= \int_0^{T_f}\int_0^{T_f} h(t)h(\tau)E[\eta_n(t)\eta_{n+k}(\tau)]d\tau dt \\
&= \sigma^2\int_0^{T_f} h(t)\int_0^{T_f} h(\tau)\cos(2\pi f_0(t-\tau-kT_f))\times B\mathrm{sinc}(B(t-\tau-kT_f))d\tau dt \\
&= \frac{\sigma^2}{2}\int_0^{T_f} h(t)\int_0^{T_f} h(\tau)\left(e^{j2\pi f_0(t-\tau-kT_f)}+e^{-j2\pi f_0(t-\tau-kT_f)}\right)\times\int_{-B/2}^{B/2} e^{j2\pi f(t-\tau-kT_f)}df d\tau dt \\
&= \frac{\sigma^2}{2}\int_0^{T_f} h(t)\left(\int_{-f_0-B/2}^{-f_0+B/2} H(f)e^{j2\pi f(t-kT_f)}df + \int_{f_0-B/2}^{f_0+B/2} H(f)e^{j2\pi f(t-kT_f)}df\right)dt \quad (37)
\end{aligned}$$

sequently, the three noise terms $\{\zeta_1, \zeta_2, \zeta_3\}$ can be treated as mutually uncorrelated. As $\zeta_3(n)$ contains the product of two uncorrelated Gaussian noise components, the central limit theorem asserts that it will also be approximately Gaussian as a consequence of the integration and summation. Since $\tilde{h}(t)$ and $\eta_n(t)$ are both zero mean, $\zeta_3(n)$ also has zero mean, and its autocorrelation function is given by (41), shown at the bottom of the page. Notice that the two sinc functions in (41) are offset by kT_f. Recalling that $T_f \gg 1/B$, we deduce that $\mathrm{sinc}(B(t-\tau))\mathrm{sinc}(B(t-\tau-kT_f)) \approx \mathrm{sinc}^2(B(t-\tau))\delta(k)$, and (41) becomes

$$E[\zeta_3(n)\zeta_3(n+k)] \approx \delta(k)\sigma^2\sigma_{\tilde{h}}^2 \times \int_0^{T_f}\int_0^{T_f} [B\mathrm{sinc}(B(t-\tau))\cos(2\pi f_0(t-\tau))]^2\, d\tau dt. \quad (42)$$

Since $T_f \gg 1/B$, applying Parseval's theorem to (42) yields

$$E[\zeta_3(n)\zeta_3(n+k)] \approx \sigma^2\sigma_{\tilde{h}}^2 \int_0^{T_f}\int_{-B/2}^{B/2} 2\left(\frac{1}{2}\right)^2 df\, dt\, \delta(k) = \frac{\sigma^2\sigma_{\tilde{h}}^2}{2} BT_f\, \delta(k). \quad (43)$$

In other words, $\zeta_3(n)$ is also approximately white Gaussian.

APPENDIX II
PROOF OF PROPOSITION 2

For fixed total information energy $\mathcal{E}_s$, and information block length N_s, we are going to show that equi-powered information symbols, i.e., $\mathcal{E}_s(n_s) = \mathcal{E}_s/N_s, \forall n_s \in [0, N_s-1]$, maximize the instantaneous capacity C_i. Defining the instantaneous capacity corresponding to the n_sth symbol as

$$C(n_s) := p(n_s)\log_2 p(n_s) + (1-p(n_s))\log_2(1-p(n_s)) + 1$$

we have

$$C_i := \sum_{n_s=0}^{N_s-1} C(n_s). \quad (44)$$

We will first show that when $N_s = 2$, C_i is maximized by setting $\mathcal{E}_s(0) = \mathcal{E}_s(1) = \mathcal{E}_s/2$. Suppose C_i is maximized when $\mathcal{E}(0) = \lambda\mathcal{E}_s$ and $\mathcal{E}(1) = (1-\lambda)\mathcal{E}_s$ with $0 \le \lambda \le 0.5$. As the summands in (44) are nonnegative, the energy distribution scheme that maximizes $C_i := \sum_{n_s=0}^{2} C(n_s)$ must satisfy the following condition.

The composite instantaneous capacity of any two out of the three symbols, namely $C(n_{s1}) + C(n_{s2})$, $n_{s1} \neq n_{s2} \in [0, 1, 2]$, is maximized, subject to their total energy $\mathcal{E}(n_{s1}) + \mathcal{E}(n_{s2})$.

Proof of this condition is straightforward, and is omitted here. The resulting optimal energy distribution scheme for $N_s = 3$ is then given by

$$\mathcal{E}(n_{s1}) : \mathcal{E}(n_{s2}) = \lambda : (1-\lambda)$$
$$\text{or } \mathcal{E}(n_{s1}) : \mathcal{E}(n_{s2}) = (1-\lambda) : \lambda,\ \forall n_{s1} \neq n_{s2} \in [0, 1, 2]$$

where $a : b$ denotes the ratio of a to b. Starting (arbitrarily) from $n_{s1} = 0$ and $n_{s2} = 1$, and letting $\mathcal{E}(0) : \mathcal{E}(1) = \lambda : (1-\lambda)$, we have the following possibilities:

A. If $\mathcal{E}(1) : \mathcal{E}(2) = \lambda : (1-\lambda)$, then $\mathcal{E}(0) : \mathcal{E}(2) = \lambda^2 : (1-\lambda)^2$. Recalling that $\mathcal{E}(0) : \mathcal{E}(2) = \lambda : (1-\lambda)$ is also required, we have $\lambda = 0$, or $\lambda = 0.5$.

B. $\mathcal{E}(1) : \mathcal{E}(2) = (1-\lambda) : \lambda$, then $\mathcal{E}(0) : \mathcal{E}(2) = 1$. Recalling that $\mathcal{E}(0) : \mathcal{E}(2) = \lambda : (1-\lambda)$ is also required, we have $\lambda = 0.5$.

Changing the order of the three symbols will yield the same results due to their rotating symmetry. Therefore, the optimal λ when $N_s = 2$ is either 0, or 0.5. Now it suffices to show that C_i associated with $\lambda = 0.5$ is no less than that associated with $\lambda = 0$ for all $\{\mathcal{E}_s, \mathcal{E}_p\}$ pairs.

For the $N_s = 2$ case, to show the dependence of $\rho_{\text{eff}}(n_s)$ and C_i on λ explicitly, we denote them with $\rho_{\text{eff}}^{(\lambda)}(n_s)$ and $C_i^{(\lambda)}$, respectively. Rearranging terms in (13), we have

$$\begin{cases} \rho_{\text{eff}}^{(0)}(0) = 0 \\ \rho_{\text{eff}}^{(0)}(1) = \frac{\mathcal{E}_s}{(\mathcal{E}_h\mathcal{E}_p + BT_f\sigma^2) + \mathcal{E}_h\mathcal{E}_s} \cdot \frac{2\mathcal{E}_h^2\mathcal{E}_p}{\sigma^2} := \rho_1 \\ \text{and} \\ \rho_{\text{eff}}^{(0.5)}(0) = \frac{\mathcal{E}_s}{2(\mathcal{E}_h\mathcal{E}_p + BT_f\sigma^2) + \mathcal{E}_h\mathcal{E}_s} \cdot \frac{2\mathcal{E}_h^2\mathcal{E}_p}{\sigma^2} := \rho_2 \\ \rho_{\text{eff}}^{(0.5)}(1) = \rho_2. \end{cases} \quad (45)$$

Accordingly, we also have

$$C_i^{(0)}(\rho_1) = p_1\log_2 p_1 + (1-p_1)\log_2(1-p_1) + 1$$

for $\lambda = 0$, where $p_1 := Q\left(\sqrt{\rho_1}\right)$; while for $\lambda = 0.5$, with $p_2 := Q\left(\sqrt{\rho_2}\right)$, we have

$$C_i^{(0.5)}(\rho_2) = 2\left[p_2\log_2 p_2 + (1-p_2)\log_2(1-p_2) + 1\right]. \quad (46)$$

It is evident from (45) that $\rho_2 \ge 0.5\rho_1$ for any given $\mathcal{E}_h$, $\mathcal{E}_p$, T_f, N_f, σ^2, and $\mathcal{E}_s$. Therefore, $p_2 \le Q\left(\sqrt{0.5\rho_1}\right) \le 0.5$ must

$$E[\zeta_3(n)\zeta_3(n+k)] = E\left[\int_0^{T_f}\int_0^{T_f} \tilde{h}(t)\eta_n(t)\tilde{h}(\tau)\eta_{n+k}(\tau)d\tau dt\right] = B^2\sigma^2\sigma_{\tilde{h}}^2 \int_0^{T_f}\int_0^{T_f} \cos(2\pi f_0(t-\tau-kT_f))\cos(2\pi f_0(t-\tau)) \times \mathrm{sinc}(B(t-\tau))\mathrm{sinc}(B(t-\tau-kT_f))d\tau dt \quad (41)$$

be true $\forall \rho_1,\ \rho_2$. Replacing p_2 in (46) with $\bar{p}_2 := Q\left(\sqrt{0.5\rho_1}\right)$ results in a lower bound of $C_i^{(0.5)}(\rho_2)$

$$\underline{C}_i^{(0.5)}(\rho_1) = 2\left[\bar{p}_2 \log_2 \bar{p}_2 + (1-\bar{p}_2)\log_2(1-\bar{p}_2) + 1\right].$$

If $\underline{C}_i^{(0.5)}(\rho_1) \geq C_i^{(0)}(\rho_1)$, $\forall \rho_1$, then $C_i^{(0.5)}(\rho_2) \geq C_i^{(0)}(\rho_1)$ must also hold true for all $\{\mathcal{E}_s, \mathcal{E}_p\}$ pairs.

As ρ_1 increases, both $\bar{p}_2$ and p_1 decrease. Therefore, both $\underline{C}_i^{(0.5)}(\rho_1)$ and $C_i^{(0)}(\rho_1)$ increase monotonically with increasing ρ_1. Also notice that the maximum of $C_i^{(0)}(\rho_1)$ is one, and is reached as ρ_1 goes to infinity. Consequently, once $\underline{C}_i^{(0.5)}(\rho_1)$ exceeds one, it will always be greater than $C_i^{(0)}(\rho_1)$. In other words, we have

$$\underline{C}_i^{(0.5)}(\rho_1) > C_i^{(0)}(\rho_1),\ \forall \rho_1 > 3.008 \approx 5\ \text{dB} \qquad (47)$$

where 5 dB is obtained by solving $\underline{C}_i^{(0.5)}(\rho_1) = 1$ for ρ_1.

What is left to show is that $\underline{C}_i^{(0.5)}(\rho_1) > C_i^{(0)}(\rho_1)$ within the region $\rho_1 < 5$ dB. To do so, we parse this region into several segments and show that $\underline{C}_i^{(0.5)}(\rho_1) - C_i^{(0)}(\rho_1)$ is lower bounded by zero over each of these segments. Noticing that $C_i^{(0)}(0) = \underline{C}_i^{(0.5)}(0) < C_i^{(0)}(3.008) < \underline{C}_i^{(0.5)}(3.008)$, the segment parsing algorithm proceeds as follows:

S1. Initialization: set $n = 1$, let $\rho_l = 0$ and $\rho_u(n) = 3.008$.
S2. Comparison: if $\rho_u(n) = \rho_l$, then stop; if not, go to S3.
S3. Updating: find $\rho_t(n) \in (\rho_l, \rho_u(n))$ that satisfies $\underline{C}_i^{(0.5)}(\rho_t(n)) = C_i^{(0)}(\rho_u(n))$, set $n = n+1$, and let $\rho_u(n) = \rho_t(n-1)$. Go to S2.

Notice that since $\underline{C}_i^{(0.5)}(\rho_1)$ is monotonically increasing, there must exist one and only one $\rho_t(n) \in (\rho_l, \rho_u(n))$ that satisfies $\underline{C}_i^{(0.5)}(\rho_t(n)) = C_i^{(0)}(\rho_u(n))$. It follows that

$$\underline{C}_i^{(0.5)}(\rho_1) - C_i^{(0)}(\rho_1) > \underline{C}_i^{(0.5)}(\rho_t(n)) - C_i^{(0)}(\rho_u(n)) = 0$$

for all $\rho_1 \in [\rho_t(n), \rho_u(n)]$. In other words, $\underline{C}_i^{(0.5)}(\rho_1) - C_i^{(0)}(\rho_1)$ is lower bounded by zero on each segment $[\rho_t(n), \rho_u(n)]$. Consequently, we have

$$\underline{C}_i^{(0.5)}(\rho_1) > C_i^{(0)}(\rho_1),\ \forall \rho_1 < 5\ \text{dB} \qquad (48)$$

which, together with (47), establishes that $C_i^{(0.5)}(\rho_2) > C_i^{(0)}(\rho_1)$, $\forall \rho_1$. As a result, $\lambda = 0.5$ is indeed optimal when $N_s = 2$. In other words, equi-powered symbols maximize C_i when $N_s = 2$. This can be readily generalized to arbitrary N_s by noticing that any two out of the N_s symbols must be equi-powered. In conclusion, equi-powered symbols maximize C_i, subject to fixed total energy $\mathcal{E}_s$ and block length N_s.

ACKNOWLEDGMENT

The authors wish to thank Dr. A. Swami of the Army Research Laboratory for his comments on the conference version of this paper. This work was prepared through collaborative participation in the Communications and Networks Consortium sponsored by the U.S. Army Research Laboratory under the Collaborative Technology Alliance Program, Cooperative Agreement DAAD19-01-2-0011.

REFERENCES

[1] S. Adireddy, L. Tong, and H. Viswanathan, "Optimal placement of training for frequency-selective block-fading channels," *IEEE Trans. Inform. Theory*, vol. 48, pp. 2338–2353, Aug. 2002.
[2] J. K. Cavers, "An analysis of pilot symbol assisted modulation for Rayleigh fading channels," *IEEE Trans. Veh. Technol.*, vol. 40, pp. 686–693, Nov. 1991.
[3] J. D. Choi and W. E. Stark, "Performance of ultra-wideband communications with suboptimal receivers in multipath channels," *IEEE J. Select. Areas Commun.*, vol. 20, pp. 1754–1766, Dec. 2002.
[4] J. R. Foerster, "The effects of multipath interference on the performance of UWB systems in and indoor wireless channel," in *Proc. Vehicular Technology Conf.*, vol. 2, Rhodes Island, Greece, 2001, pp. 1176–1180.
[5] J. R. Foerster, E. Green, S. Somayazulu, and D. Leeper. (2001) Ultra-wideband technology for short or medium range wireless communications. *Intel Technol. J. Q2* [Online]. Available: http://intel.com/technology/itj/q22001/pdf/art_4.pdf
[6] "Technical Information Series," G.E. Research and Development Center, Jan. 2002.
[7] S. M. Kay, *Fundamentals of Statistical Signal Processing, Volume I: Estimation Theory*, 1st ed. Englewood Cliffs, NJ: Prentice-Hall, 1993.
[8] H. Lee, B. Han, Y. Shin, and S. Im, "Multipath characteristics of impulse radio channels," in *Proc. Vehicular Technology Conf. Proc.*, Tokyo, Japan, 2000, pp. 2487–2491.
[9] C. J. Le Martret and G. B. Giannakis, "All-digital impulse radio for wireless cellular systems," *IEEE Trans. Commun.*, vol. 50, pp. 1440–1450, Sept. 2002.
[10] V. Lottici, A. D'Andrea, and U. Mengali, "Channel estimation for ultra-wideband communications," *IEEE J. Select. Areas Commun.*, vol. 20, pp. 1638–1645, Dec. 2002.
[11] J. Proakis, *Digital Communications*, 4th ed. New York: McGraw-Hill, 2001.
[12] S. Ohno and G. B. Giannakis, "Optimal training and redundant precoding for block transmissions with application to wireless OFDM," *IEEE Trans. Commun.*, vol. 50, pp. 2113–2123, Dec. 2002.
[13] A. A. M. Saleh and R. A. Valenzuela, "A statistical model for indoor multipath propagation," *IEEE J. Select. Areas Commun.*, vol. JSAC-5, pp. 128–137, Feb. 1987.
[14] R. A. Scholtz, "Multiple access with time-hopping impulse radio," in *Proc. Milcom Conf.*, Boston, MA, Oct. 1993, pp. 447–450.
[15] M. K. Simon *et al.*, *Spread Spectrum Communications Handbook*. New York: McGraw-Hill, 1985.
[16] J. D. Taylor, *Introduction to Ultra-Wideband Systems*. Ann Arbor, MI: CRC Press, 1995.
[17] Z. Tian, L. Yang, and G. B. Giannakis, "Symbol timing estimation in ultra-wideband communications," in *Proc. 36th Asilomar Conf. Signals, Systems, and Computers*, Pacific Grove, CA, Nov. 3–6, 2002.
[18] M. L. Welborn, "System considerations for ultra-wideband wireless networks," in *IEEE Radio Wireless Conf.*, Boston, MA, Aug. 2001, pp. 5–8.
[19] M. Z. Win and R. A. Scholtz, "On the energy capture of ultrawide bandwidth signals in dense multipath environments," *IEEE Commun. Lett.*, vol. 2, pp. 245–247, Sept. 1998.
[20] ——, "Ultra wide bandwidth time-hopping spread-spectrum impulse radio for wireless multiple access communications," *IEEE Trans. Commun.*, vol. 48, pp. 679–691, 2000.
[21] L. Yang and G. B. Giannakis, "Multi-stage block-spreading for impulse radio multiple access through ISI channels," *IEEE J. Select. Areas Commun.*, vol. 20, pp. 1767–1777, Dec. 2002.
[22] L. Yang, Z. Tian, and G. B. Giannakis, "Non-data aided timing acquisition of ultra-wideband transmissions using cyclostationarity," in *Proc. Int. Conf. Acoustics, Speech and Signal Processing*, Hong Kong, Apr. 6–10, 2003.

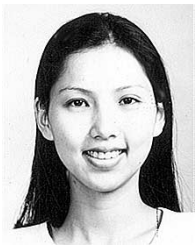

Liuqing Yang (S'02) received the B.S. degree in electrical engineering from Huazhong University of Science and Technology, Wuhan, China, in 1994, and the M.Sc. and Ph.D. degrees in electrical and computer engineering from the University of Minnesota, Minneapolis, in 2002 and 2004, respectively.

Her research interests include communications, signal processing and networking. Currently, she has a particular interest in ultrawideband (UWB) communications. Her research encompasses synchronization, channel estimation, equalization, multiple access, space-time coding, and multicarrier systems.

Georgios B. Giannakis (S'84–M'86–SM'91–F'97) received the Diploma in electrical engineering from the National Technical University of Athens, Greece, 1981, and the MSc. degree in electrical engineering, the MSc. degree in mathematics, and the Ph.D. degree in electrical engineering, from the University of Southern California (USC), Los Angeles, in 1983, 1986, and 1986, respectively.

After lecturing for one year at USC, he joined the University of Virginia in 1987, where he became a Professor of Electrical Engineering in 1997. Since 1999, he has been a Professor with the Department of Electrical and Computer Engineering at the University of Minnesota, Minneapolis, where he now holds an ADC Chair in Wireless Telecommunications. His general interests span the areas of communications and signal processing, estimation and detection theory, time-series analysis, and system identification—subjects on which he has published more than 160 journal papers, 300 conference papers, and two edited books. His current research focuses on transmitter and receiver diversity techniques for single-user and multiuser fading communication channels, complex-field and space–time coding, multicarrier, ultrawideband wireless communication systems, cross-layer designs, and distributed sensor networks.

Dr. Giannakis is the (co-) recipient of four best paper awards from the IEEE Signal Processing (SP) Society (1992, 1998, 2000, 2001). He also received the Society's Technical Achievement Award in 2000. He co-organized three IEEE-SP Workshops, and guest (co-) edited four special issues. He has served as Editor in Chief for the IEEE SIGNAL PROCESSING LETTERS, as Associate Editor for the IEEE TRANSACTIONS ON SIGNAL PROCESSING and the IEEE SIGNAL PROCESSING LETTERS, as Secretary of the SP Conference Board, as Member of the SP Publications Board, as Member and Vice-chair of the Statistical Signal and Array Processing Technical Committee, and as Chair of the SP for Communications Technical Committee. He is a Member of the Editorial Board for the PROCEEDINGS OF THE IEEE, and the steering committee of the IEEE TRANSACTIONS ON WIRELESS COMMUNICATIONS.